Relativistic decay widths of autoionization processes: The relativistic FanoADC-Stieltjes method

Elke Fasshauer, Přemysl Kolorenč, and Markus Pernpointner

Articles you may be interested in

Ab initio interatomic decay widths of excited states by applying Stieltjes imaging to Lanczos pseudospectra
J. Chem. Phys. **134**, 094107 (2011); 10.1063/1.3558739

Autoionization widths by Stieltjes imaging applied to Lanczos pseudospectra
J. Chem. Phys. **134**, 024106 (2011); 10.1063/1.3523982

The Auger (Autoionization) Decay of Excited States in Spectra of Multicharged Ions: Relativistic Theory
AIP Conf. Proc. **1290**, 94 (2010); 10.1063/1.3517587

Large-scale parallel configuration interaction. I. Nonrelativistic and scalar-relativistic general active space implementation with application to (Rb – Ba) +
J. Chem. Phys. **128**, 014108 (2008); 10.1063/1.2805369

Recent development of self-interaction-free time-dependent density-functional theory for nonperturbative treatment of atomic and molecular multiphoton processes in intense laser fields
J. Chem. Phys. **123**, 062207 (2005); 10.1063/1.1904587

Relativistic decay widths of autoionization processes: The relativistic FanoADC-Stieltjes method

Elke Fasshauer,[1,2,a)] Přemysl Kolorenč,[3] and Markus Pernpointner[2]

[1]*Centre for Theoretical and Computational Chemistry, Department of Chemistry, University of Tromsø–The Arctic University of Norway, N-9037 Tromsø, Norway*
[2]*Theoretische Chemie, Universität Heidelberg, Im Neuenheimer Feld 229, D-69120 Heidelberg, Germany*
[3]*Institute of Theoretical Physics, Faculty of Mathematics and Physics, Charles University in Prague, V Holešovičkách 2, 180 00 Prague, Czech Republic*

Electronic decay processes of ionized systems are, for example, the Auger decay or the Interatomic/Intermolecular Coulombic Decay. In both processes, an energetically low lying vacancy is filled by an electron of an energetically higher lying orbital and a secondary electron is instantaneously emitted to the continuum. Whether or not such a process occurs depends both on the energetic accessibility and the corresponding lifetime compared to the lifetime of competing decay mechanisms. We present a realization of the non-relativistically established FanoADC-Stieltjes method for the description of autoionization decay widths including relativistic effects. This procedure, being based on the Algebraic Diagrammatic Construction (ADC), was adapted to the relativistic framework and implemented into the relativistic quantum chemistry program package Dirac. It is, in contrast to other existing relativistic atomic codes, not limited to the description of autoionization lifetimes in spherically symmetric systems, but is instead also applicable to molecules and clusters. We employ this method to the Auger processes following the $Kr3d^{-1}$, $Xe4d^{-1}$, and $Rn5d^{-1}$ ionization. Based on the results, we show a pronounced influence of mainly scalar-relativistic effects on the decay widths of autoionization processes. © *2015 AIP Publishing LLC.* [http://dx.doi.org/10.1063/1.4917255]

I. INTRODUCTION

Electronic vacancies in the sub-outer-valence orbital of an atom or molecule created by radiation or radioactive decay are excited systems. These excited systems can decay via multiple pathways like photon emission, coupling to vibrational degrees of freedom or via electronic decay processes like the Auger decay,[1,2] or the manifold of Interatomic/Intermolecular Coulombic Decay (ICD) processes,[3,4] both being autoionization processes. The latter can occur in small[5–7] and large[4,8–11] noble gas clusters, as well as clusters of molecules like water,[12–16] ammonia,[17] or hydrogen fluoride[3,18] after exposure to synchrotron radiation, in enzymes of the human body,[19] in the mechanisms of cancer drugs,[20–25] and quantum dots in semiconductors[26] just to name a few examples.

Electronic decay processes in general can occur if two criteria, the energy and the coupling criterion, are fulfilled. To fulfill the energy criterion, the final state energy is required to be lower than the energy of the singly ionized initial state. If this is not the case, the channel defined by a certain doubly ionized final state is closed and the corresponding fragments of the channel are not observed after the decay. To fulfill the coupling criterion, the decay process needs to be fast enough to prevail over other energetically accessible decay pathways. It hence contains the information whether an energetically allowed process can be expected to be observed experimentally or not. Therefore, a typical study of autoionization processes consists of two parts.

- Determination of the kinetic energy of the secondary electron and, as a consequence, which decay channels are open.
- Calculation of the decay width $\Gamma = \frac{\hbar}{\tau}$, which is proportional to the decay rate $\frac{1}{\tau}$ and inversely proportional to the lifetime τ.

Especially in systems containing heavy elements or initial ionizations from the core region, relativistic effects play an important role and cannot be neglected. Phenomenologically, the relativistic effects can be divided into spin-orbit coupling and scalar-relativistic effects. The spin-orbit coupling requires the system to be described in terms of the total angular momentum j rather than the orbital momentum l and the spin momentum s. Thereby, the non-relativistically degenerate states of one particular l value are split into two states with $j = l \pm s$ of different energies.[27] The scalar-relativistic effects result in spatial contractions of the s and p orbitals and decontraction of d and f orbitals.[27]

Spin-orbit coupling has been shown to cause a larger number of distinguishable channels in ICD-like processes.[28] At the same time, the influence of the spin-orbit splitting using asymptotic formulas based on experimental data of the atoms was investigated. The results showed only minor deviations of the decay widths due to spin-orbit coupling in the case of all channels being open. However, this approach intrinsically includes scalar-relativistic effects, which are automatically included in the experimental data used. In order to investigate also the influence of scalar-relativistic effects and to enable a relativistic description at short bond distances, the

a)Email: Elke.Fasshauer@uit.no

142, 144106-1

purpose of this paper is to present the *ab initio* relativistic FanoADC-Stieltjes method for the determination of decay widths. From our calculations, we gain further insights into the influence of relativistic (mainly scalar-relativistic) effects on Auger processes and from these, generalize our findings for autoionization processes.

In both autoionization processes (Auger and ICD), the initial vacancy is filled with an electron of higher energy and the excess energy is transferred to another electron, which is finally emitted. Hence, the final state is characterized by a doubly charged system and an electron in the continuum. Our subject of interest is mainly the ICD-like processes. However, due to the similarity between the autoionization processes, methods developed for the description of ICD-like processes can also be applied to the Auger process, where more data from theory and experiment are available for comparison.

In this work, we therefore focus on the atomic Auger process as a model system in order to exploit basic knowledge about the influence of relativistic effects. The Auger decay process initiated by a photoionization can most generally be described by

$$A \xrightarrow{h\nu} (A^+)^* + e^-_{ph} \xrightarrow{Auger} A^{2+} + e^-_{ph} + e^-_{sec}.$$
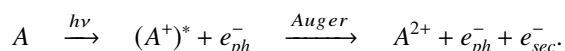
A system A is ionized, while the photo-electron e^-_{ph} is emitted. Afterwards, the actual Auger process of the initial state A^+ can occur. An electron from an outer shell fills the vacancy and the excess energy is instantaneously transferred to another (secondary) electron e^-_{sec}, which is subsequently emitted. The final state of the decay process is to be described by a doubly charged atom A^{2+} and the secondary electron in the continuum.

The initial and final state energies can be obtained using a variety of quantum chemical approaches known in the literature as the Algebraic Diagrammatic Construction[29–32] (ADC), which is also available for a fully relativistic treatment.[33–35] On the other hand, the evaluation of decay widths Γ is a highly non-trivial problem. Analytically, it can be described by the theories of Feshbach and Fano.[36–38] However, this theory naturally incorporates the description of both bound and continuum states, which describe the initial and final state, respectively. These different kinds of states satisfy different boundary conditions, i.e., the boundary conditions of bound states being of $\mathcal{L}^2$-type and the boundary conditions of plane waves in case of the final state because of the freely moving electron. Any approach will have to stick to either $\mathcal{L}^2$-functions, plane waves or to combine these two in some way connecting the bound with the continuum functions. Either of these approaches faces difficulties in either describing the bound or the continuum states or some artificially constructed interface region.

It is most convenient to start from an $\mathcal{L}^2$-function based approach, because most quantum chemical programs are based on this kind of functions and hence the basic ingredients necessary for a decay width calculation like SCF and integral transformation are already available. The quantum chemical methods, which have been used for non-relativistic descriptions of the decay widths are the Wigner-Weisskopf theory,[39] CAP-CI (Complex Absorbing Potential

based on a Configuration Interaction wavefunction),[6,40] CAP-ADC,[41] CAP/EOM-CCSD (Equation of Motion Coupled Cluster with Singles and Doubles)[42] and the FanoADC-Stieltjes method.[43] While the CAP-based methods have the most sound formal basis of the methods above, they suffer from wrong densities and populations for many-particle systems and are computationally expensive at the same time. In contrast to this, the Wigner-Weisskopf theory is based on the lowest non-vanishing order of perturbation theory and therefore computationally affordable even for large systems. However, the price for the lower computational costs is less accurate results. A compromise between accuracy and computational cost is the FanoADC-Stieltjes approach, which is based on the ADC and therefore includes higher perturbational orders and is size-consistent. For these reasons, the FanoADC-Stieltjes method was implemented in the relativistic quantum chemical program package Dirac.[44] We present first results obtained with the relativistic FanoADC-Stieltjes method in this work.

So far, relativistic decay widths were calculated using Multichannel Multi-Configurational Dirac-Fock (MMCDF).[45] However, this approach does not only highly depend on manual selection of CI (Configuration Interaction) components to be included in the description of initial and final state, it moreover is not capable of describing systems with less than spherical symmetry. This reduces the applicability of the method to atomic Auger processes, but allows us to compare our results obtained with the relativistic FanoADC-Stieltjes method for exactly this special case.

Based on the results for the Auger process following the $(n-1)d^{-1}$ ionization of the noble gases krypton, xenon, and radon, we are going to show the importance of including relativistic effects into decay width calculations based on comparisons of four-component Dirac-Coulomb (including spin-orbit coupling and scalar-relativistic effects), scalar-relativistic, and non-relativistic results.

The paper is structured as follows: in Sec. II, we explain the physical definition of the decay widths and the three compounds of the FanoADC-Stieltjes method: ADC, FanoADC, and Stieltjes imaging. We then give the computational details for our *ab initio* calculations in Sec. III and present our results for the Auger process after an initial ionization of the $(n-1)$d of krypton, xenon, and radon. We discuss the influence of relativistic effects on the decay widths of autoionization processes in Sec. IV. We then draw conclusions in Sec. V.

II. THEORY

Following Wentzel[46] and later Feshbach[36,38] and Fano,[37] the decay width of a decay process initiated by a primary ionization is given by

$$\Gamma = \sum_{\beta} 2\pi \left| \langle \Phi | \hat{V} | \chi_{\beta,\varepsilon} \rangle \right|^2. \tag{1}$$

Here, $|\Phi\rangle$ and $|\chi_{\beta,\varepsilon}\rangle$ denote the initial and final state, respectively. $\hat{V}$ is the interaction operator of the initial and final states, which in Feshbach's definitions is known as H_{PQ}. The index β counts the different decay channels and ε denotes the energy of the final state. Equation (1) thereby connects the metastable initial and the continuum final states.

They are constructed by partitioning the Hamiltonian into two subspaces. The initial (final) state is then an eigenfunction of this initial (final) state sub-space Hamiltonian. However, finding proper solutions to both the initial and the final states on an equal footing is a non-trivial task, because they adhere to different boundary conditions. Since the final state depends on the energy of the emitted electron, any approach needs to either determine the continuum state or to mimic the final state using $\mathcal{L}^2$-functions. While the continuum functions are normalized with respect to their energy,

$$\langle \chi_\varepsilon | \chi_{\varepsilon'} \rangle = \delta(\varepsilon - \varepsilon'), \tag{2}$$

the $\mathcal{L}^2$ approach is based on a discrete set of final states $|\tilde{\chi}_{\tilde{E}}\rangle$ which adhere to different boundary conditions and are normalized with respect to space (see, e.g., Ref. 47),

$$\langle \tilde{\chi}_{\tilde{E}_i} | \tilde{\chi}_{\tilde{E}_j} \rangle = \delta_{ij}. \tag{3}$$

Because of this different normalization, the decay widths are not amenable to a direct calculation. As first proposed by Hazi,[48] for autoionization processes such difficulties can be solved by using the Stieltjes-Chebyshev moment theory also called Stieltjes imaging.[49–51] It relies on the observation that the moments of the projected final state Hamiltonian H_f,

$$\mu_k = \langle \Phi | \hat{V} H_f^k \hat{V} | \Phi \rangle, \tag{4}$$

calculated from the determined discrete pseudo-spectrum are good approximations to the moments determined from the real continuum states. This can be shown by inserting the resolution of identity for the continuum states

$$\mu_k = \sum_i \varepsilon_i^k \left| \langle \Phi | \hat{V} | \chi_{i,\varepsilon} \rangle \right|^2 + \int_{E_{thr}}^\infty \varepsilon^k \left| \langle \Phi | \hat{V} | \chi_\varepsilon \rangle \right|^2 d\varepsilon. \tag{5}$$

Since the non-zero contribution to the coupling matrix elements in the Feshbach-Fano approach stems only from an interaction region of finite size, where the $\mathcal{L}^2$ final state functions are nonvanishing, we may replace the expansion $\sum_i |\chi_{i,\varepsilon}\rangle\langle\chi_{i,\varepsilon}| + \int d\varepsilon |\chi_\varepsilon\rangle\langle\chi_\varepsilon|$ by its $\mathcal{L}^2$ approximation $\sum_j |\tilde{\chi}_{\tilde{E}_j}\rangle\langle\tilde{\chi}_{\tilde{E}_j}|$ (see Ref. 52),

$$\mu_k \approx \sum_j \tilde{E}_j^k \left| \langle \Phi | \hat{V} | \tilde{\chi}_{\tilde{E}_j} \rangle \right|^2. \tag{6}$$

Then the decay width can be determined through a series of consecutive approximations to the moments of increasing order k.

To achieve this kind of description, we choose the non-relativistic FanoADC-Stieltjes approach, described in Secs. II A–II C. Here, the ADC is used for the description of the initial and final states and the resulting discrete pseudo-spectrum is then subject to a Stieltjes imaging procedure. An exhaustive description of the method can be found in Ref. 53.

A. ADC

The ADC is a Green's function approach, which is a method for the calculation of ionization energies and electron affinities. Its advantage is the ability to determine the desired ionization energies without explicit calculation of the initial and final states, but instead obtaining their energy differences

directly. Moreover, this approach is size-consistent and is hence suitable for the description of larger systems.[32]

Originally, the Green's function was formulated in the Dyson ansatz and determined using perturbation theory.[29,54] This way, both the ionization and the electron affinity part had to be included in the description. In the non-Dyson scheme, those two are separable and hence, the dimension of the problem is reduced when one is interested in either the $N + 1$ (electron affinity) or the $N - 1$ (ionization energy) part[31]

$$G_{pq}(\omega) = G_{pq}^+(\omega) + G_{pq}^-(\omega). \tag{7}$$

The ionization part $G_{pq}^-(\omega)$ is a function of the ionization energies ω and is transposed to give $\tilde{G}_{pq}^-(\omega) = G_{qp}^-(\omega)$. It can be cast to the compact and orthogonal form

$$\tilde{\mathbf{G}}^-(\omega) = \mathbf{x}^\dagger (\omega \mathbb{1} - \mathbf{\Omega})^{-1} \mathbf{x}, \tag{8}$$

where $\mathbf{x}$ are the spectroscopic amplitudes and $\mathbf{\Omega}$ is the diagonal matrix of energy eigenvalues. This diagonal representation can be reformulated using so-called *intermediate states* (IS),[30]

$$\tilde{\mathbf{G}}^-(\omega) = \mathbf{f}^\dagger (\omega \mathbb{1} - \mathbf{M})^{-1} \mathbf{f}. \tag{9}$$

Here, $\mathbf{M}$ denotes the ADC matrix and $\mathbf{f}$ denotes the effective transition moments.

By inspection of both Eqs. (8) and (9), the ionization energies are poles of $\tilde{\mathbf{G}}^-(\omega)$, which can be determined by solving the eigenvalue problem

$$\mathbf{MY} = \mathbf{Y\Omega}, \quad \text{with } \mathbf{Y}^\dagger \mathbf{Y} = \mathbf{1}. \tag{10}$$

The spectroscopic amplitudes $\mathbf{x}$ can then be obtained from the effective transition moments $\mathbf{f}$ as

$$\mathbf{x} = \mathbf{Y}^\dagger \mathbf{f}. \tag{11}$$

To this point, the approach is exact. For the actual construction of the ADC matrix $\mathbf{M}$ and the effective transitions moments $\mathbf{f}$, both are expanded into orders of perturbations based on the Møller-Plesset partitioned Hamiltonian,

$$\mathbf{M} = \mathbf{M}^{(0)} + \mathbf{M}^{(1)} + \mathbf{M}^{(2)} + \cdots, \tag{12}$$

$$\mathbf{f} = \mathbf{f}^{(0)} + \mathbf{f}^{(1)} + \mathbf{f}^{(2)} + \cdots. \tag{13}$$

From these, different orders of perturbation theory of the Hamiltonian can be constructed successively in terms of correlated $N - 1$ particle states ($1h$, $2h1p$, ...). Hereby, the truncation after the n-th order leads to ADC(n). The contributions to the different classes for different orders of ADC are shown in Figure 1.[55]

The matrix elements of ADC(2x) are explicitly given by

- $1h/1h$ ($1h$ block):

$$M_{kk'}^{(0)} = \varepsilon_k \delta_{kk'}, \tag{14}$$

$$M_{kk'}^{(1)} = 0, \tag{15}$$

$$M_{kk'}^{(2)} = -\frac{1}{2} \sum_{abl} V_{ab[kl]} V_{k'l[ab]}$$
$$\times \frac{\varepsilon_a + \varepsilon_b - \varepsilon_l - \frac{1}{2}\varepsilon_k - \frac{1}{2}\varepsilon_{k'}}{(\varepsilon_a + \varepsilon_b - \varepsilon_k - \varepsilon_l)(\varepsilon_a + \varepsilon_b - \varepsilon_{k'} - \varepsilon_l)}. \tag{16}$$

FIG. 1. Schematic illustration of an ADC(n) matrix for different orders of perturbation for $n = 0, 1, 2, 2x, 3$. In the illustration, the respective highest order contribution is shown for the different blocks. Hence, ADC(2x) is an extended ADC(2) including first order contributions to the satellite block.

- $1h/2h1p$ (coupling block):

$$M^{(1)}_{j,akl} = V_{kl[aj]}. \tag{17}$$

- $2h1p/2h1p$ (satellite block):

$$M^{(0)}_{akl,a'k'l'} = (-\varepsilon_a + \varepsilon_k + \varepsilon_l)\, \delta_{aa'}\delta_{kk'}\delta_{ll'}, \tag{18}$$

$$M^{(1)}_{akl,a'k'l'} = -\delta_{aa'}V_{k'l'[kl]} + \delta_{kk'}V_{al'[a'l]} \\ + \delta_{ll'}V_{ak'[a'k]} - (k \leftrightarrow l). \tag{19}$$

Here, ε_r denotes the r-th Hartree Fock orbital energy. The occupied states are labelled by $i, j, k, \ldots$ and the unoccupied states are labelled by $a, b, c, \ldots$. The two-electron integrals for any combination of occupied and unoccupied orbitals labelled by p, q, r, s read as

$$V_{pqrs} = \langle \varphi_p(1)\varphi_q(2)|V(1,2)|\varphi_r(1)\varphi_s(2)\rangle \tag{20}$$

and $V_{pq[rs]} = V_{pqrs} - V_{pqsr}$.

These equations can also be used in the relativistic case based on Dirac-Hartree-Fock orbital energies as well as integrals[33,34] and using the no-pair approximation (see, e.g., Ref. 27). This approximation ensures that pair creation processes are excluded from the calculation by allowing annihilation and creation operators c_p and $c_q^\dagger$ in the spectral representation

$$G^-_{pq}(\omega) = \sum_{n\in\{N-1\}} \frac{\langle \Psi_0^N | c_q^\dagger | \Psi_n^{N-1} \rangle \langle \Psi_n^{N-1} | c_p | \Psi_0^{N-1} \rangle}{\omega + E_n^{N-1} - E_0^N - i\eta} \tag{21}$$

of Eq. (7) to operate on the space of positive energy solutions only. Since energies high enough to overcome the gap of $2mc^2$ are hardly achieved in chemistry, this approximation is reasonable.

B. FanoADC

In the FanoADC, the discrete ADC Hamiltonian is used for the construction of the pseudo-spectrum of the total decay width Γ. Due to multiple possible final states, the procedure of Feshbach[38] using projection operators for the partitioning of the Hamiltonian into an initial and a final state subspace

is employed. The processes of interest start from a singly ionized initial state and end in a doubly ionized final state with an additional electron in the continuum. Therefore, the basis functions for the description of the entire final state subspace are chosen from the $2h1p$ class of configurations, where the $2h$ part is assumed to describe the doubly ionized final state and the particle represents the electron in the continuum. This approach can be justified by rewriting the spectral moments (see Eq. (6)) of the decay width Γ (Eq. (1)) explicitly

$$\tilde{\Gamma}_k = 2\pi\mu_k \tag{22}$$

$$= 2\pi \sum_j \tilde{E}_j^k \langle \Phi|\hat{V}|\tilde{\chi}_{\tilde{E}_j}\rangle \langle \tilde{\chi}_{\tilde{E}_j}|\hat{V}|\Phi\rangle \tag{23}$$

$$\approx 2\pi \sum_q \left(E_q^{2h1p}\right)^k \langle \Phi|\hat{V}|\chi_q^{2h1p}\rangle \langle \chi_q^{2h1p}|\hat{V}|\Phi\rangle. \tag{24}$$

One may interpret the set of final states as a complete basis of the final state subspace. This might be replaced by any other complete basis describing the outgoing electron. The idea of the FanoADC is to choose the manifold of $2h1p$ states describing the decay to replace this complete basis. As shown in Ref. 43, this basis is not required to yield the exact energies of the different channels as long as it spans the space of interest. The manifold of $2h1p$ states is formally not complete, but yields a proper description when the ionization of the system can be described reasonably well in the single-particle picture. Additionally, one has to consider the error introduced by using an incomplete basis set on the Hartree-Fock level and the truncation of the virtual space in the post Hartree-Fock procedure.

Not all $2h1p$ states describe energetically allowed final states. The energy conservation $E_{in} = E_{A^{2+}} + E_{e^-_{sec}}$ has to be satisfied, which is only possible for $E_{A^{2+}} < E_{in}$, where E_{in} denotes the initial state energy, $E_{A^{2+}}$ the energy of the doubly ionized part of the final state, and $E_{e^-_{sec}}$ denotes the kinetic energy of the secondary electron emitted in the process. If the energy of the doubly charged system is higher than the energy of the initial state, the process is energetically forbidden. Hence, all $2h1p$ states characterized by a $2h$ contribution with an energy higher than the initial state energy will not contribute to the final states. Instead, these $2h1p$ states can be used to improve the description of the initial state. The partitioning into initial and final state configurations can be achieved based on Hartree-Fock orbital occupations by manual choice of $2h$ configurations or in an energy-based approach as described by Averbukh.[43] In this work, we employ the partitioning by population and manually include those configurations which correspond to open channels.

The partitioning is therefore achieved as follows. All $2h1p$ configurations characterized by a $2h$ part corresponding to one of the final state configurations of possible decay channels are chosen to be part of the final state subspace. All $1h$ configurations and those $2h1p$ configurations not corresponding to a possible final state configuration are used for the description of the initial state. This leads to a resorted ADC matrix as shown in Figure 2, where the subspace of the initial state is denoted by **M**, the final state subspace by **N**, and the interaction coupling those two subsets is named **W**.
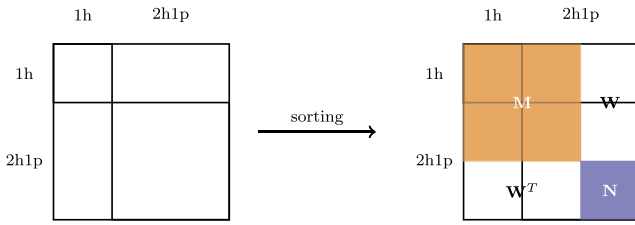
FIG. 2. Schematic illustration of the partitioning of the ADC matrix according to the projection operators of the initial and final states.

Speaking in terms of Feshbach's projection operators, where **P** denotes the projector for the final state subspace acting on the full Hamiltonian of the system **H** and $\mathbf{Q} = \mathbb{1} - \mathbf{P}$ denotes the projector for the initial state subspace, these subspaces are given by $\mathbf{M} = \mathbf{QHQ}$ and $\mathbf{N} = \mathbf{PHP}$.

The separate diagonalization of the initial and final state subspaces **M** and **N** yields the corresponding eigenvectors and eigenvalues on the diagonal of the matrices $\mathbf{\Lambda}$ and $\mathbf{\Omega}$,

$$\mathbf{\Lambda} = \mathbf{I}^T \mathbf{M} \mathbf{I}, \tag{25}$$

$$\mathbf{\Omega} = \mathbf{F}^T \mathbf{N} \mathbf{F}, \tag{26}$$

and the Hamiltonian is represented in the basis of their eigenstates as illustrated in Figure 3 with $\mathbf{V} = \mathbf{I}^T \mathbf{W} \mathbf{F}$ being the interaction part in this new basis. It has to be noticed that $\mathbf{\Omega}$ in this definition is the matrix of final state subspace eigenvalues and does not equal the eigenvalue matrix of the full ADC matrix in Eq. (8).

In general, neither of the final state energies $\bar{\omega}_q$ equals the resonance energy. Therefore, the pseudo-spectrum enters the Stieltjes calculation. For a specific choice of the initial state i, this pseudo-spectrum is given by the manifold of final state energies $\bar{\omega}_q$ and the corresponding interaction part in the basis of the initial and final subspace eigenstates $V_{i,q} = \langle \phi_i | \hat{V} | \psi_q^{2h1p} \rangle$.

C. Stieltjes imaging

In general, Gaussian quadrature is a numerical method to solve integrals. From the discrete pseudo-spectrum consisting of $\bar{\omega}_q$ and $V_{i,q} = \langle \phi_i | \hat{V} | \psi_q^{2h1p} \rangle$, N pairs of optimal abscissae $(1/\omega_i)$ and weights f_i for a Gaussian quadrature can be obtained using Chebyshev polynomials as elaborately described in Ref. 51. These are then used for the construction of inverse moments, which are preferred to normal moments because of their convergence behaviour

$$S(-k) = \int_{E_{thr}}^{\infty} \omega^{-k} \, dF(\omega) = \int_{E_{thr}}^{\infty} \omega^{-k} f(\omega) \, d\omega$$

$$\approx \sum_{i=1}^{N} \left(\frac{1}{\omega_i} \right)^k f_i. \tag{27}$$

The inverse moments are in terms of Gaussian quadrature connected to both the distribution function $F(\omega)$ and a density function $f(\omega)$. In the particular case of interest, the density function $f(\omega)$ equals the decay width $\Gamma(E)$ (see Eq. (6)). The procedure and the background shortly explained here can be found in detail in Refs. 49, 50, 52, and 56. For convenience, we from this point on write the optimal abscissae $\frac{1}{\omega_i}$ as ε.

Having obtained the optimal abscissae and weights, the probability distribution function $F(\varepsilon)$ can be approximated. For this purpose, the so-called Stieltjes imaging is employed, where

$$F^{(n)}(\varepsilon) = \begin{cases} 0 & \varepsilon < \varepsilon_1 \\ \sum_{j=1}^{i} f_j & \varepsilon_i < \varepsilon < \varepsilon_{i+1} \\ \sum_{j=1}^{n} f_j = S(0) & \varepsilon_n < \varepsilon. \end{cases} \tag{28}$$

This procedure is based on the so-called Chebyshev inequalities

$$F^{(n)}(\varepsilon_i - 0) \le F^{(n+1)}(\varepsilon_i - 0) \le F(\varepsilon_i) \le F^{(n+1)}(\varepsilon_i + 0)$$

$$\le F^{(n)}(\varepsilon_i + 0). \tag{29}$$

This means that the distribution functions obtained from the Chebyshev polynomials approaching the abscissae ε_i from below and from above give lower and upper bounds to the actual value of the distribution function at this particular point $F(\varepsilon_i)$. In fact, the mean of these two values usually is a very good approximation to the exact value

$$F^{(n)}(\varepsilon_i) = \frac{1}{2} \left[F^{(n)}(\varepsilon_i - 0) + F^{(n)}(\varepsilon_i + 0) \right]. \tag{30}$$

Since the integral was evaluated and not the density function, as such the distribution function obtained from the discrete pseudo-spectrum is normalized correctly (see Ref. 52). This distribution function is then numerically differentiated via

$$f^{(n)}(\varepsilon) = \begin{cases} \dfrac{1}{2} \dfrac{f_1}{\varepsilon_1} & \varepsilon < \varepsilon_1 \\ \dfrac{1}{2} \dfrac{f_{i+1} + f_i}{\varepsilon_{i+1} - \varepsilon_i} & \varepsilon_i < \varepsilon < \varepsilon_{i+1} \\ 0 & \varepsilon_n < \varepsilon \end{cases} \tag{31}$$
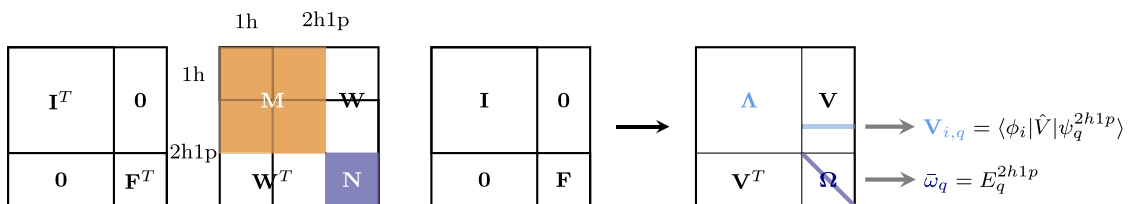

FIG. 3. Schematic illustration of the basis transformation of the full ADC matrix into the basis of initial and final states. The pseudo-spectrum is given by the manifold of $\bar{\omega}_q$ and $V_{i,q} = \langle \phi_i | \hat{V} | \psi_q^{2h1p} \rangle$.

to give $r - 1$ non-zero points of the desired density function $f(\varepsilon)$, which are subsequently interpolated. In the routine of Averbukh, a monotonicity-preserving piecewise cubic Hermite spline interpolation is used for this purpose. Afterwards, the interpolated density function is evaluated for the energy of interest, which is the resonance energy E_r in case of the autoionization processes to give the decay width Γ. Finally, convergence of the decay widths with increasing orders of moments is investigated.

Unfortunately, the procedure to obtain the optimal abscissae and weights involves the subtraction of two large numbers, which leads to numerical instabilities in high order moments. Therefore, they have to be checked carefully and only trustworthy moments should be used for the evaluation of the decay widths. This can be achieved by inspection of abscissae and weights of each order. Since the decay width $\Gamma(E)$ is a smooth function, unphysical oscillations in the curve constructed from the abscissae and weights of one order of moments indicate numerical instabilities in this particular order. If this behaviour is observed, the abscissae and weights obtained from this order of moments and all higher orders are discarded. Finally, the abscissae and weights from the remaining, consecutive orders of moments enter the interpolation scheme.

III. COMPUTATIONAL DETAILS

The decay width calculations were performed using the relativistic FanoADC-Stieltjes code, which has been implemented in Dirac.[44] For each element, four-component calculations based on the Dirac-Coulomb Hamiltonian, scalar-relativistic spin-free calculations, and non-relativistic calculations were performed. Hereby, the respective cv4z basis sets of Dyall[57] were used and diffuse basis functions of the Kaufmann-Baumeister-Jungen type[58] were added at the center of the atom. For the s, p, and d-type functions, five functions were added for each orbital type and three f-type functions were added to the basis set.

The resulting moments were checked for numerical instabilities. Only those moments without numerical instabilities entered the interpolation scheme for the determination of the decay widths.

The expectation value of the radial distance $\langle r \rangle$ and orbital densities were performed using the atomic program GRASP.[59]

IV. RESULTS AND DISCUSSION

We present theoretical values for the Kr$3d^{-1}$, Xe$4d^{-1}$, and Rn$5d^{-1}$ Auger decay widths. The relativistically calculated single and double ionization potential spectra (SIPs and DIPs) for xenon are shown in Fig. 4 as representative of the three noble gases.[33–35] A more detailed population analysis of the double ionization spectrum can be found in Ref. 60. From this, the energetically accessible Auger decay channels can be deduced by comparison of the respective spectra. All doubly ionized states with an ionization energy lower than the ionization energy of the initial $(n - 1)$d state can be populated after the decay. Hence, three major final state groups are
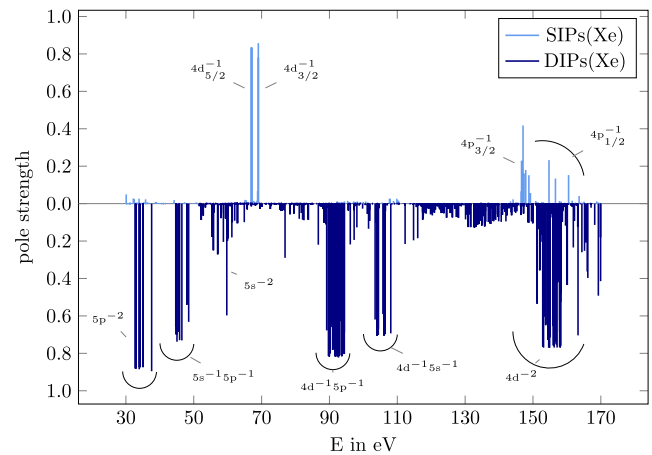

FIG. 4. Comparison of the single and double ionization spectra of the xenon atom obtained by a DC-ADC calculation. All groups of doubly ionized states with lower energies than the initially ionized Xe$4d^{-1}$ can be considered as possible final states.

found in all three cases: ns^{-2}, ns^{-1}np^{-1}, and np^{-2}. From the corresponding $2h$ configurations, the final state subspaces of the decay width calculations were constructed.

Due to truncation of the full ADC matrix caused by the partitioning into initial and final state subspaces, the absolute value of the single ionization energy of the initial state used as approximation to the real part of the resonance energy loses accuracy. Even though the discrepancies are about 1–2 eV, this shift does only have a minor effect on the resulting decay widths in the results presented here, because the density functions $\Gamma(E)$ are very flat around the resonance energy. However, this shift can in general be a source of error and results obtained with the FanoADC-Stieltjes method have to be checked carefully.

The resulting decay widths and, if available, experimental and theoretically obtained decay widths for comparison are shown in Table I.

For krypton, one other set of calculated decay widths is available in the literature.[61] These calculations are based

TABLE I. Total Auger decay widths of the Kr, Xe, and Rn Rg$(n-1)$d$_{5/2}^{-1}$, and Rg$(n-1)$d$_{3/2}^{-1}$ and the non-relativistic Rg$(n-1)$d^{-1} initial states compared to theoretical values for krypton,[61] xenon,[62] and experimental values for xenon.[63] All widths are given in meV.

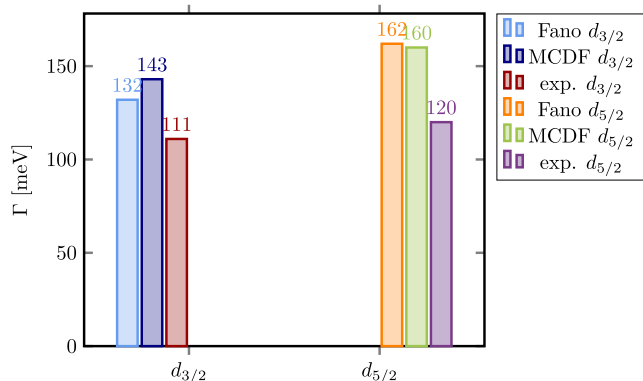| Γ	Initial state	Exp.	Theoretical	This work
	$3d_{5/2}$	...	51	63
	$3d_{3/2}$	...	49	56
Kr	$3d_{spinfree}$	...	...	62
	$3d_{nrel}$	...	...	49
	$4d_{5/2}$	110–130	160	162
	$4d_{3/2}$	105–116	143	132
Xe	$4d_{spinfree}$	...	...	168
	$4d_{nrel}$	...	...	90
	$5d_{5/2}$	...	...	624
	$5d_{3/2}$	...	...	547
Rn	$5d_{spinfree}$	...	...	686
	$5d_{nrel}$	...	...	161

FIG. 5. Comparison of the xenon Auger decay widths from the $Xe4d_{3/2}^{-1}$ and $4d_{5/2}^{-1}$ initial state obtained with the relativistic FanoADC in this work, the MMCDF approach,[62] and mean experimental values.[63] The calculated values are in very good agreement with each other, while both methods provide higher decay widths than the experimental ones.

on a many-body perturbation approach including all orders of perturbation. The authors state that these results are approximately 75% of the values for calculations including perturbations up to second order only. Therefore, the second order numbers would agree well with our values obtained with the FanoADC-Stieltjes method shown in Table I. However, all integrations in this procedure rely on analytic evaluation using angular momentum algebra and are hence not applicable to non-spherical systems.

In case of Xe, both experimental and theoretical data are available in the literature. A graphical comparison of this data to our results is shown in Figure 5. The theoretical results from Ref. 62 were obtained using the MMCDF method.[45] For quantum chemists, the name of this method might be misleading, since it is by no means equivalent to Multi-Configurational Self-Consistent Field (MCSCF). MMCDF is based on an atomic Dirac-Fock calculation. For the initial state description of the xenon decay widths in Ref. 62, the pure Dirac-Fock solution is used. For the final state description, the Dirac-Fock solution is the reference state for a CI approach. Then, the excitation classes are chosen manually based on the experience of the scientist as well as by trial and error. In the case of the xenon decay widths shown in Table I and Figure 5, $5s^05p^6$, $5s^15p^5$, and $5s^25p^4$ configurations were included in the final state description. This resembles the space spanned by the $2h1p$ states in our FanoADC-Stieltjes approach. However, the method is generally not limited to doubly ionized states but can additionally include higher order excitations as well (see, e.g., Ref. 64). Hence, results from both the FanoADC-Stieltjes approach presented in this work and the MMCDF results of Ref. 62 include dynamic correlation in the description of the final state. However, the results obtained with the FanoADC-Stieltjes method incorporate correlation effects in the initial state description as well.

Considering the different qualities of the initial state description, the results of Ref. 62 are in excellent agreement with the results obtained with the fully relativistic four-component FanoADC-Stieltjes method. Both approaches overestimate the decay width compared to experiment. Taking into account that in this non-trivial problem of the calculation
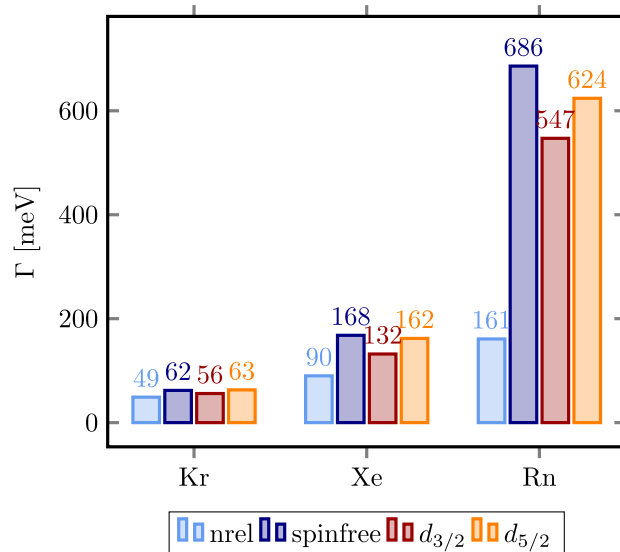

FIG. 6. Comparison of the Auger decay widths after primary ionization in the $Rg(n-1)d^{-1}$ for different Hamiltonians. The non-relativistically obtained results are lower than those obtained with the spinfree and four-component Hamiltonian. Overall, the decay width increases with the atomic number Z.

of decay widths, errors within a factor of two are to be expected, the results are in reasonably good agreement with experiment as well. Latest results of Sukhorukov indicate that the overestimation of the decay widths by both the MMCDF and the FanoADC results is due to these methods lacking the description of core polarization[65,66] first discussed by Born and Heisenberg.[67]

From Table I and Figure 6, it can be seen that only the four-component calculation is capable of describing the spin-orbit splitting which causes two different initial states. Therefore, this calculation is to be preferred. However, by employing the other schemes as well, one can learn more about the nature of the decay process.

The spinfree results with scalar-relativistic effects included are very close to the fully relativistic results for all three elements. In contrast to this, the non-relativistically obtained decay width is much smaller in all three cases. The difference increases as one goes down in the periodic table, which is summarized in Table II. In case of radon, the decay width is about four times as high as one would expect from a non-relativistic treatment.

This shows that the inclusion of at least scalar-relativistic effects is crucial in the calculation of autoionization decay widths in systems containing heavy elements. The reason for this behaviour can easily be understood, remembering that scalar-relativistic effects can phenomenologically be described as the decontraction of d and f and the contraction of s and

TABLE II. Absolute and relative increase of the decay widths due to the inclusion of scalar-relativistic effects in the calculations. The absolute decrease is given in meV.

	Kr	Xe	Rn
$\Delta_{spinfree,nrel}$	13	78	525
Increase	+27%	+87%	+326%

TABLE III. Expectation values of the electron's distance from the nucleus for the noble gases Kr, Xe, and Rn given in Å.

$\langle r \rangle$		$(n-1)\mathrm{d}_-$	$(n-1)\mathrm{d}_+$	$n\mathrm{s}$	$n\mathrm{p}_-$	$n\mathrm{p}_+$
Kr	rel	0.292	0.293	0.847	1.013	1.037
	nrel		0.291	0.862		1.033
Xe	rel	0.460	0.466	1.008	1.186	1.245
	nrel		0.460	1.048		1.237
Rn	rel	0.559	0.578	1.017	1.186	1.366
	nrel		0.561	1.141		1.346
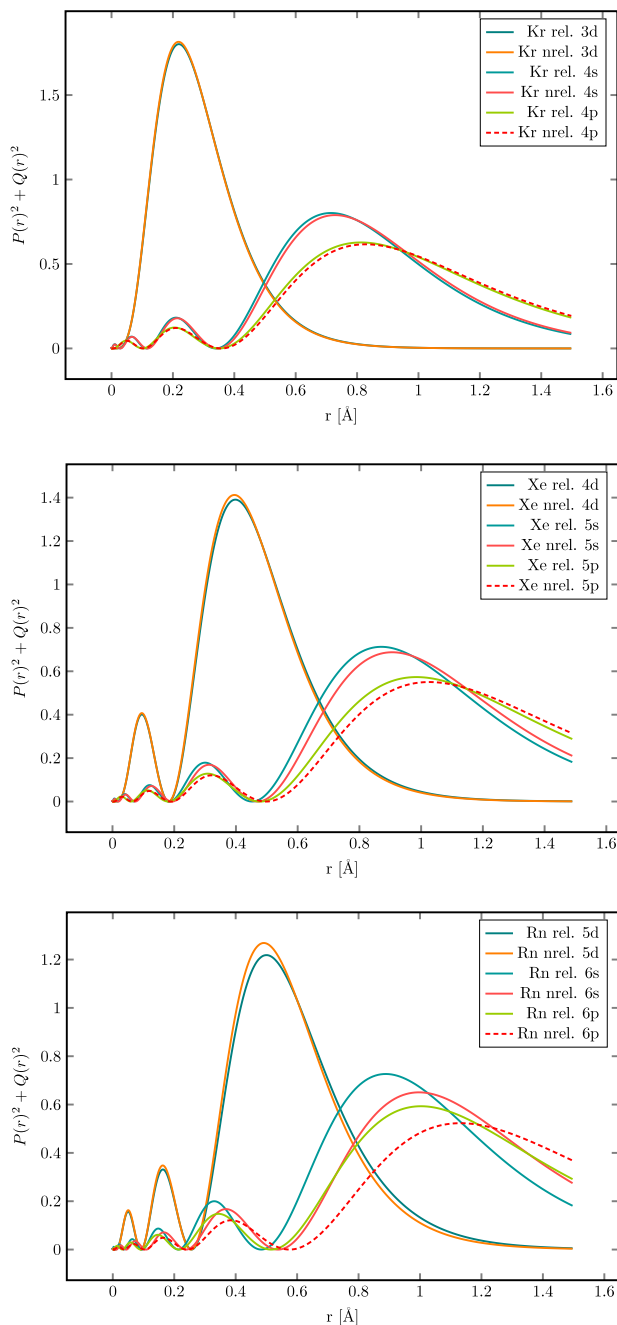
FIG. 7. Probability densities $P(r)^2 + Q(r)^2$ for the orbitals participating in the Auger decay for Kr, Xe, and Rn calculated both relativistically and non-relativistically.

p orbitals, which in this case corresponds to initial and final states, respectively (see Table III and Figure 7). It can be seen that the decontraction of the d orbitals is only minor but the contraction of especially the s orbitals and also the p orbitals is remarkable and increases within the group.

Hence, the difference $\Delta\langle r \rangle = \langle r_{in} \rangle - \langle r_{fin} \rangle$ between the distance expectation values of the electron $\langle r \rangle$ from the nucleus between the orbitals describing the initial state and those orbitals describing the final states is decreased. This leads to an increased spatial overlap between the initial and final states, which in turn influences the decay width by making the s/p → d de-excitation transition more efficient. In the case at hand, the smaller $\Delta\langle r \rangle$ leads to an increase of the decay width. Likewise, a larger $\Delta\langle r \rangle$ would lead to a decrease of the decay width compared to the non-relativistic description.

This effect does not only affect the decay widths of Auger processes but also the decay widths of many other autoionization processes like the ICD or the Electron Transfer Mediated Decay (ETMD). The latter relies on an electron transfer between two units and hence can be expected to be crucially influenced by the scalar-relativistic effects reported in this work. Both will be subject to future research.

V. CONCLUSIONS

We presented the relativistic counterpart of the non-relativistically known FanoADC-Stieltjes approach. This method is able to predict decay widths including relativistic effects also for non-spherical systems, which was not possible so far, according to our knowledge, with other approaches. The calculations of ICD decay widths using the relativistic FanoADC-Stieltjes approach are going to be subject of future work.

Decay widths for the Auger process following an initial ionization from the $(n-1)$d of krypton, xenon, and radon were calculated using three different Hamiltonians. They cover the four component approach including both spin-orbit coupling and scalar-relativistic effects, the spinfree approach only including scalar-relativistic effects and the non-relativistic approach for comparison. In the results, we observe a large influence of the scalar-relativistic effects, which increases going down in the periodic table within a group. We show that these are caused by a change in overlap of the orbitals involved in the decay mainly due to the contraction of the s and p orbitals.

We predict these findings not to be unique to Auger processes but to be a general effect in autoionization processes including ICD and ETMD. Therefore, we propose further investigation of ICD and ETMD processes in systems containing heavy elements. The systems of interest for this purpose are systems with initially ionized d orbitals and final states containing vacancies in s orbitals. Also, the inverse setup with the initial vacancy in an s orbital and final states containing d vacancies can be expected to show the influence of relativistic effects. These effects are expected to be larger in ETMD than in ICD processes. However, due to the large computational cost growing with system size, one would start to study the ICD process.

ACKNOWLEDGMENTS

[1]L. Meitner, Z. Phys. **9**, 131 (1922).

[2]P. Auger, C. R. Acad. Sci. **177**, 169 (1923).

[3]L. S. Cederbaum, J. Zobeley, and F. Tarantelli, Phys. Rev. Lett. **79**, 4778 (1997).

[4]S. Marburger, O. Kugeler, U. Hergenhahn, and T. Möller, Phys. Rev. Lett. **90**, 4 (2003).

[5]J. Zobeley, R. Santra, and L. S. Cederbaum, J. Chem. Phys. **115**, 5076 (2001).

[6]R. Santra, J. Zobeley, and L. S. Cederbaum, Phys. Rev. B **64**, 245104 (2001).

[7]S. Scheit, V. Averbukh, H.-D. Meyer, N. Moiseyev, R. Santra, T. Sommerfeld, J. Zobeley, and L. S. Cederbaum, J. Chem. Phys. **121**, 8393 (2004).

[8]T. Jahnke, A. Czasch, M. S. Schöffler, S. Schössler, A. Knapp, M. Käsz, J. Titze, C. Wimmer, K. Kreidi, R. E. Grisenti, A. Staudte, O. Jagutzki, U. Hergenhahn, H. Schmidt-Böcking, and R. Dörner, Phys. Rev. Lett. **93**, 4 (2004).

[9]G. Öhrwall, M. Tchaplyguine, M. Lundwall, R. Feifel, H. Bergersen, T. Rander, A. Lindblad, J. Schulz, S. Peredkov, S. Barth, S. Marburger, U. Hergenhahn, S. Svensson, and O. Björneholm, Phys. Rev. Lett. **93**, 173401 (2004).

[10]M. Lundwall, W. Pokapanich, H. Bergersen, A. Lindblad, T. Rander, G. Öhrwall, M. Tchaplyguine, S. Barth, U. Hergenhahn, S. Svensson, and O. Björneholm, J. Chem. Phys. **126**, 214706 (2007).

[11]E. Fasshauer, M. Förstel, S. Pallmann, M. Pernpointner, and U. Hergenhahn, New J. Phys. **16**, 103026 (2014).

[12]I. B. Müller and L. S. Cederbaum, J. Chem. Phys. **125**, 204305 (2006).

[13]S. D. Stoychev, A. I. Kuleff, and L. S. Cederbaum, J. Chem. Phys. **133**, 154307 (2010).

[14]P. Slavíček, B. Winter, L. S. Cederbaum, and N. V. Kryzhevoi, J. Am. Chem. Soc. **136**, 18170 (2014).

[15]T. Jahnke, H. Sann, T. Havermeier, K. Kreidi, C. Stuck, M. Meckel, M. Schöffler, N. Neumann, R. Wallauer, S. Voss, A. Czasch, O. Jagutzki, A. Malakzadeh, F. Afaneh, T. Weber, H. Schmidt-Böcking, and R. Dörner, Nat. Phys. **6**, 139 (2010).

[16]M. Mucke, M. Braune, S. Barth, M. Förstel, T. Lischke, V. Ulrich, T. Arion, U. Becker, A. Bradshaw, and U. Hergenhahn, Nat. Phys. **6**, 143 (2010).

[17]N. V. Kryzhevoi and L. S. Cederbaum, Angew. Chem., Int. Ed. **50**, 1306 (2011).

[18]J. Zobeley, L. S. Cederbaum, and F. Tarantelli, J. Chem. Phys. **108**, 9737 (1998).

[19]P. H. P. Harbach, M. Schneider, S. Faraji, and A. Dreuw, J. Phys. Chem. Lett. **4**, 943 (2013).

[20]E. Surdutovich and A. V. Solov'yov, Eur. Phys. J. D **66**, 206 (2012).

[21]H.-K. Kim, J. Titze, M. Schöffler, F. Trinter, M. Waitz, J. Voigtsberger, H. Sann, M. Meckel, C. Stuck, U. Lenz, M. Odenweller, N. Neumann, S. Schössler, K. Ullmann-Pfleger, B. Ulrich, R. Costa Fraga, N. Petridis, D. Metz, A. Jung, R. Grisenti, A. Czasch, O. Jagutzki, L. Schmidt, T. Jahnke, H. Schmidt-Böcking, and R. Dörner, Proc. Natl. Acad. Sci. U. S. A. **108**, 11821 (2011).

[22]U. Hergenhahn, Int. J. Radiat. Biol. **88**, 871 (2012).

[23]B. Boudaïffa, P. Cloutier, D. Hunting, M. A. Huels, and L. Sanche, Science **287**, 1658 (2000).

[24]X. Pan, P. Cloutier, D. Hunting, and L. Sanche, Phys. Rev. Lett. **90**, 208102 (2003).

[25]F. Martin, P. D. Burrow, Z. Cai, P. Cloutier, D. Hunting, and L. Sanche, Phys. Rev. Lett. **93**, 068101 (2004).

[26]A. Bande, K. Gokhberg, and L. S. Cederbaum, J. Chem. Phys. **135**, 144112 (2011).

[27]M. Reiher and A. Wolf, *Relativistic Quantum Chemistry* (Wiley-VCH Verlag GmbH, 2009).

[28]E. Fasshauer, M. Pernpointner, and K. Gokhberg, J. Chem. Phys. **138**, 014305 (2013).

[29]J. Schirmer, Phys. Rev. A **26**, 2395 (1982).

[30]J. Schirmer, Phys. Rev. A **43**, 4647 (1991).

[31]J. Schirmer, A. B. Trofimov, and G. Stelter, J. Chem. Phys. **109**, 4734 (1998).

[32]F. Mertins and J. Schirmer, Phys. Rev. A **53**, 2140 (1996).

[33]M. Pernpointner and A. B. Trofimov, J. Chem. Phys. **120**, 4098 (2004).

[34]M. Pernpointner, J. Chem. Phys. **121**, 8782 (2004).

[35]M. Pernpointner, J. Phys. B **43**, 205102 (2010).

[36]H. Feshbach, Ann. Phys. **5**, 357 (1958).

[37]U. Fano, Phys. Rev. **124**, 1866 (1961).

[38]H. Feshbach, Ann. Phys. **19**, 287 (1962).

[39]R. Santra and L. S. Cederbaum, Phys. Rep. **368**, 117 (2002).

[40]J. J. Sakurai, in *Modern Quantum Mechanics*, rev. ed., edited by S. F. Tuan (Addison-Wesley, 1994).

[41]N. Vaval and L. S. Cederbaum, J. Chem. Phys. **126**, 164110 (2007).

[42]A. Ghosh, N. Vaval, S. Pal, and R. J. Bartlett, J. Chem. Phys. **141**, 164113 (2014).

[43]V. Averbukh and L. S. Cederbaum, J. Chem. Phys. **123**, 204107 (2005).

[44]DIRAC, a relativistic *ab initio* electronic structure program, Release DIRAC13 (2013), written by L. Visscher, H. J. Aa. Jensen, R. Bast, and T. Saue, with contributions from V. Bakken, K. G. Dyall, S. Dubillard, U. Ekström, E. Eliav, T. Enevoldsen, E. Faßhauer, T. Fleig, O. Fossgaard, A. S. P. Gomes, T. Helgaker, J. K. Lærdahl, Y. S. Lee, J. Henriksson, M. Iliaš, Ch. R. Jacob, S. Knecht, S. Komorovský, O. Kullie, C. V. Larsen, H. S. Nataraj, P. Norman, G. Olejniczak, J. Olsen, Y. C. Park, J. K. Pedersen, M. Pernpointner, K. Ruud, P. Sałek, B. Schimmelpfennig, J. Sikkema, A. J. Thorvaldsen, J. Thyssen, J. van Stralen, S. Villaume, O. Visser, T. Winther, and S. Yamamoto (see http://www.diracprogram.org).

[45]S. Fritzsche, A. N. Grum-Grzhimailo, E. V. Gryzlova, and N. M. Kabachnik, J. Phys. B **44**, 175602 (2011).

[46]G. Wentzel, Z. Phys. **43**, 524 (1927).

[47]J. Craigie, A. Hammad, B. Cooper, and V. Averbukh, J. Chem. Phys. **141**, 014105 (2014).

[48]A. Hazi, J. Phys. B **11**, L259 (1978).

[49]P. W. Langhoff, C. T. Corcoran, F. Sims, J. S. Weinhold, and R. M. Glover, Phys. Rev. A **14**, 1042 (1976).

[50]C. T. Corcoran and P. W. Langhoff, J. Math. Phys. **18**, 651 (1977).

[51]F. Müller-Plathe and G. H. F. Diercksen, *Electronic Structure of Atoms, Molecules and Solids* (Kluwer Academic Publishers, 1990).

[52]W. P. Reinhardt, Comput. Phys. Commun. **17**, 1 (1979).

[53]E. Fasshauer, "Investigation of relativistic effects in electronic decay processes in small and large noble gas clusters by *ab initio* and new simulation approaches," Ph.D. thesis (University of Heidelberg, 2014).

[54]J. Schirmer, L. S. Cederbaum, and O. Walter, Phys. Rev. A **28**, 1237 (1983).

[55]A. B. Trofimov and J. Schirmer, J. Chem. Phys. **123**, 144115 (2005).

[56]F. Müller-Plathe and G. H. F. Diercksen, Phys. Rev. A **40**, 696 (1989).

[57]K. G. Dyall, Theor. Chem. Acc. **115**, 441 (2006).

[58]K. Kaufmann, W. Baumeister, and M. Jungen, J. Phys. B **22**, 2223 (1989).

[59]F. A. Parpia, C. Froese Fischer, and I. P. Grant, Comput. Phys. Commun. **94**, 249 (1996).

[60]M. Pernpointner, J. P. Zobel, and N. V. Kryzhevoi, Phys. Rev. A **85**, 012205 (2012).

[61]J. C. Baggesen, E. Lindroth, and L. B. Madsen, Phys. Rev. A **85**, 013415 (2012).

[62]A. Mäntykenttä, Phys. Rev. **47**, 3961 (1993).

[63]A. Ausmees, A. Hahlin, S. L. Sorensen, S. Sundin, I. Hjelte, O. Björneholm, and S. Svensson, J. Phys. B **32**, 197 (1999).

[64]S. Heinäsmäki, H. Aksela, J. Nikkinen, E. Kukk, A. Kivimäki, S. Aksela, and S. Fritzsche, J. Electron Spectrosc. Relat. Phenom. **137–140**, 281 (2004).

[65]I. D. Petrov, B. M. Lagutin, V. L. Sukhorukov, A. Ehresmann, and H. Schmoranzer, J. Phys. B **47**, 055001 (2014).

[66]V. L. Sukhorukov, I. D. Petrov, M. Schäfer, F. Merkt, M.-W. Ruf, and H. Hotop, J. Phys. B **45**, 092001 (2012).

[67]M. Born and W. Heisenberg, Z. Phys. **23**, 388 (1924).